

Simulated hydrogen diffusion in diamond grain boundaries

J.A. Pittard^{a,*}, M.Y. Lavrentiev^b, N.A. Fox^a

^a School of Physics, HH Wills Physics Laboratory, University of Bristol, Tyndall Avenue, Bristol BS8 1TL, UK

^b UKAEA, Culham Campus, Abingdon OX14 3DB, UK

ARTICLE INFO

Keywords:

Diamond
Grain boundary
Diffusion
Molecular dynamics
Hydrogen

ABSTRACT

To evaluate hydrogen diffusion within diamond, a series of molecular dynamics simulations have been carried out in which diffusion coefficients and activation energies were determined. Diamond grown via chemical vapour deposition (CVD) contains a high hydrogen concentration within grain boundaries, because of this, common tilt grain boundaries were recreated from transmission electron microscopy images taken from literature. Diffusion coefficients of hydrogen placed within the grain boundary were estimated and compared to the bulk diffusion. Unlike many crystalline structures, some grain boundaries presented limited diffusion when compared to the bulk. Diffusion characteristics of grain boundaries are thought to be a result of channelling effects combined with the formation of sp^3C-H bonds with sp^2 carbon present within some grain boundaries - increasing and decreasing diffusion rates respectively. Potential wells were observed across some but not all the grain boundaries resulting in hydrogen trapping and anisotropic diffusion.

1. Introduction

Both natural and lab grown diamond are known contain high levels of hydrogen impurities. In the case of diamond grown via chemical vapour deposition (CVD), hydrogen's preferential etching of sp^2 is exploited to help remove graphitic phases forming, allowing the sp^3 diamond to grow. As such, CVD diamond is grown using a hydrogen dominant gas mixture (typically ~99 % [1]) resulting in significant amounts becoming trapped in the lattice. Many of the applications of CVD diamond require an understanding of this impurity. For example, hydrogen impurities are known to alter the electrical characteristics of semiconductor devices, and for potential applications in the fusion industry the retention and transport of tritium within materials is a major consideration [2].

The vast majority of hydrogen impurities can be found within the grain boundaries of polycrystalline (PC) CVD diamond [3]. As a result of this, grain boundaries could play a disproportionate role in determining hydrogen diffusion, despite the number of carbon atoms in the bulk being proportionally much higher. The diffusion characteristics of specific grain boundaries and the amount of hydrogen within will dictate the impact annealing treatments would have on hydrogen content of different grain boundaries.

CVD growth conditions will dictate the grain size of the resulting diamond. Longer growths typically result in thicker films and larger

grain sizes, decreasing the proportion of the diamond made up of grain boundaries and also changing the type of grain boundaries present. For example, in nanocrystalline diamond (NCD), grain boundary carbon atoms can make up to 10 % of the total atoms [4] with both tilt and twist boundaries present [5]. Due to the columnar growth of CVD diamond, thicker films will typically exhibit larger grains - reducing the proportion of carbon in the grain boundaries significantly and increasing the proportion of tilt grain boundaries [6].

This work focuses on four grain boundaries common to CVD diamond. Sawada et al. [7] identified atomic structures of four tilt grain boundaries (111 Σ 3, 221 Σ 9, 114 Σ 9, and 112 Σ 3) from transmission electron microscopy (TEM) images of CVD diamond. Using these images, these grain boundaries have been recreated computationally in this work. Other work [6,8–12] has also reported the presence of these grain boundaries with the 111 Σ 3 appearing most prevalent. Higher order Σ 27 and Σ 81 boundaries have also been reported but these form from the meeting of two lower order boundaries and are therefore less common.

2. Methodology

Molecular dynamics simulations were performed in LAMMPS (Large-scale Atomic/ Molecular Massively Parallel Simulator [13,14] to study the energetics and atomic structure of diamond grain boundaries, as well

* Corresponding author.

E-mail address: jp17358@bristol.ac.uk (J.A. Pittard).

<https://doi.org/10.1016/j.diamond.2024.111665>

Received 12 August 2024; Received in revised form 28 September 2024; Accepted 12 October 2024

Available online 13 October 2024

0925-9635/© 2024 Published by Elsevier B.V.

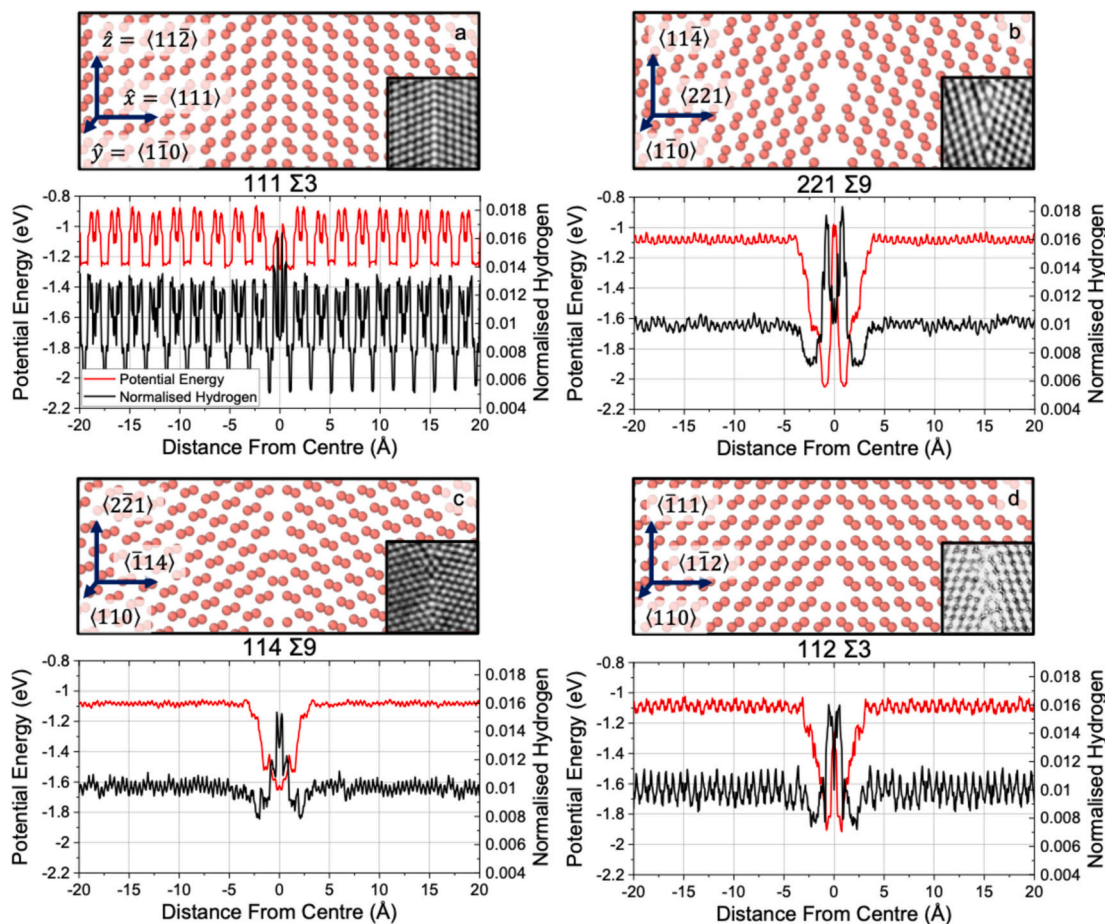


Fig. 1. Atomic structures of four tilt grain boundaries – 111 Σ 3, 221 Σ 9, 114 Σ 9 and 112 Σ 3 (labelled a, b, c and d respectively). All structures pictured contain no hydrogen atoms and are orientated with $\langle 110 \rangle$ into the page (y -axis). In the plots below, the red line shows the potential energy along the x -axis of hydrogen placed randomly within the structure and minimised. The black line shows the final positions of these hydrogen atoms, this has been normalised by the total hydrogen added across the hole structure (not just ± 20 Å from the grain boundary as shown here). The same scale has been used on all axes to aid comparison. Transmission electron microscopy (TEM) images of the replicated structure are also included (taken from [7]). Rendered in Ovito [21].

as the diffusion of hydrogen within. For all simulations and energy minimisations, the Adaptive Intermolecular Reactive Empirical Bond Order (AIREBO [15–17]) potential was used to dictate carbon carbon and carbon hydrogen interactions. For systems containing a grain boundary, it was orientated perpendicular to x (aligned with the yz plane). Periodic boundary conditions were used in all dimensions - simulating larger grain boundary planes in y and z , and a second grain boundary at the edge of the simulation cell in x . A variable timestep was used that ensured a single atom could not change kinetic energy by >100 eV or move >0.1 Å in a single timestep. The default timestep was 1 fs. The temperature was controlled by sampling from an isothermal-isobaric (NpT) ensemble with a temperature damping parameter of 1 ps and no external pressure applied.

Tilt grain boundaries from TEM images taken from [7] were recreated by creating new unit cells (UCs) of the desired orientations. These UCs maintained flat faces in x , y and z directions and were orientated to align the target grain boundary plane with x . For each grain boundary, the new UC was replicated out to a size of approximately $28 \times 57 \times 57$ Å (equivalent to $8 \times 16 \times 16$) standard diamond UCs) to make one grain, and then again to make a second, mirrored, grain which could be placed next to the first to form a twinned grain boundary. Total system size was approximately $57 \times 57 \times 57$ Å but did vary between the different structures due to the discrete size of the UCs used to produce them. The gap between the grains was selected through considering the expected sp^3 -C-C bond length (1.54 Å), total system energy post minimisation and the displacement of atoms during this minimisation. These methods

were broadly in agreement, in any case, the difference this gap makes is expected to be minimal, as the temperature in the diffusion simulations was controlled by sampling from an isothermal-isobaric (NpT) ensemble meaning the system volume, and therefore the grain boundary gap, could vary. Replicating out orientated UCs ensured periodic boundary conditions could be maintained at the boundary. It has been suggested that removing random atoms from within the grain boundary can achieve lower system energies [18,19]. Although, others have reported this made minimal difference [20], suggesting any benefit may be grain boundary specific. It was not deemed necessary to deploy this method as significant potential wells were already observed across the grain boundaries and structures were in good agreement with the TEM images they are reproducing.

A series of simulations were carried out to map the potential energy of hydrogen within the diamond. To do this, hydrogen atoms were created in random positions within the simulation box prior to performing an energy minimisation to allow atoms to reach stable positions. The number of atoms added was varied to correspond to 1 at.%, this was to reduce hydrogen hydrogen interactions and distortion of the structure whilst minimising the number of simulations required to collect sufficient data. This process was repeated 500–800 times, to give a total of around 138,000–264,800 hydrogen atoms depending on the grain boundary. To give the hydrogen positions and potential energy along a certain direction, hydrogen atoms within a 0.5 Å slice were counted and the potential energy of these atoms averaged. The bounds of this slice moved along x in 0.05 Å increments until the entire cell had

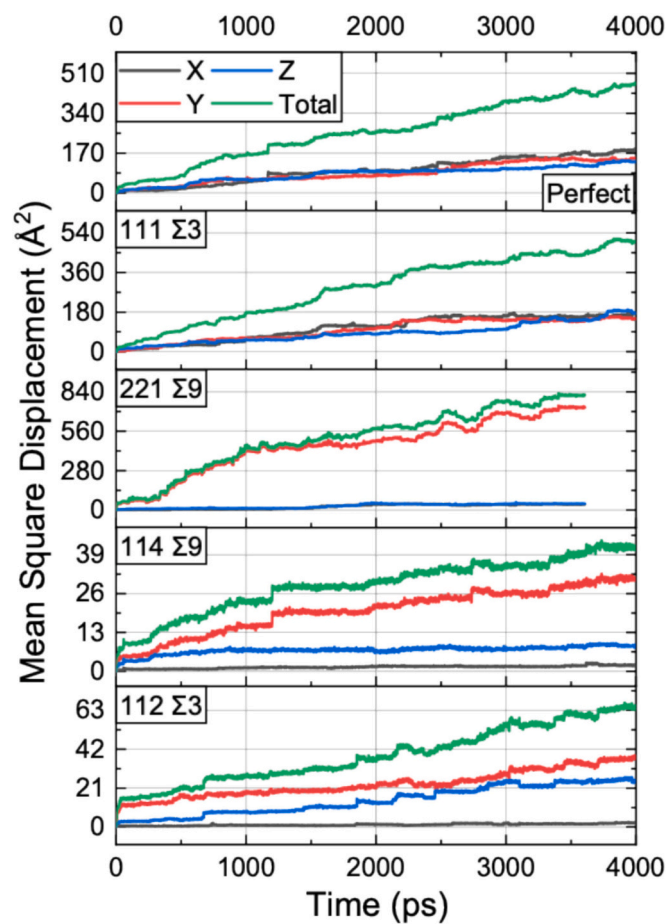


Fig. 2. Raw mean square displacement (MSD) values for hydrogen diffusing in different diamond structures at a temperature of 2750 K. Miller indices in the legend indicate orientation of faces meeting in the grain boundary (GB) along x . The perfect diamond contained no grain boundary. All structures were orientated with $\langle 110 \rangle$ direction aligned with y . Diffusion coefficients were taken as the gradient of a linear fit on total MSD divided by 6 (Eq. 1).

been covered. Heatmaps of the potential energy in two dimensions where also produced.

In order to measure diffusion, 25 hydrogen atoms were created in both grain boundaries (50 in total) in each simulation box. The grain boundary planes were split into a grid with boxes of $2 \times 2 \text{ \AA}$ in size. Hydrogen atoms were created in random positions within each of these boxes to ensure even separation. A similar process was used for evaluating bulk diffusion coefficients with a block of perfect diamond.

An energy minimisation was then performed, before a run of approximately 4 ns at an elevated temperature (ranging between 1500 and 3125 K). Diffusion coefficients were estimated from hydrogen mean-square displacement (MSD) values. Plotting MSD as a function of time, t , gives a gradient of six times the diffusion coefficient, D , as

$$\text{MSD} = 6Dt \quad (1)$$

D varies as a function of temperature, T , according to the Arrhenius law.

$$D(T) = D_0 e^{-E_A/RT} \quad (2)$$

Therefore, plotting the log of D as a function of reciprocal temperature should give a linear gradient from which activation energy, E_A , can be estimated.

Various methods were used to explore carbon hybridisations present within the structures. Coordination numbers (CN) are commonly used [22] to distinguish between different carbon hybridisations and were calculated using a 1.73 \AA cutoff distance. Atoms within this distance were classed as nearest neighbours and were used to calculate bond lengths and angles. Although bonds were not explicitly modelled, bond lengths were taken to be the distance between two nearest neighbours, and bond angles the angle between the displacement vectors of two pairs of nearest neighbours.

Changes in hybridisation on the addition of hydrogen to the grain boundaries were also explored. To do this, 100 hydrogen atoms were added randomly between both grain boundaries (up to 5 at.% within the grain boundaries) in each simulation box and the system was minimised. For the 114 grain boundary (GB), only 50 hydrogen atoms were added in an attempt to minimise disorder. Depending on the grain boundary, these minimisations were repeated 10–50 times, with hydrogen in different positions for each repeat. As coordination number will

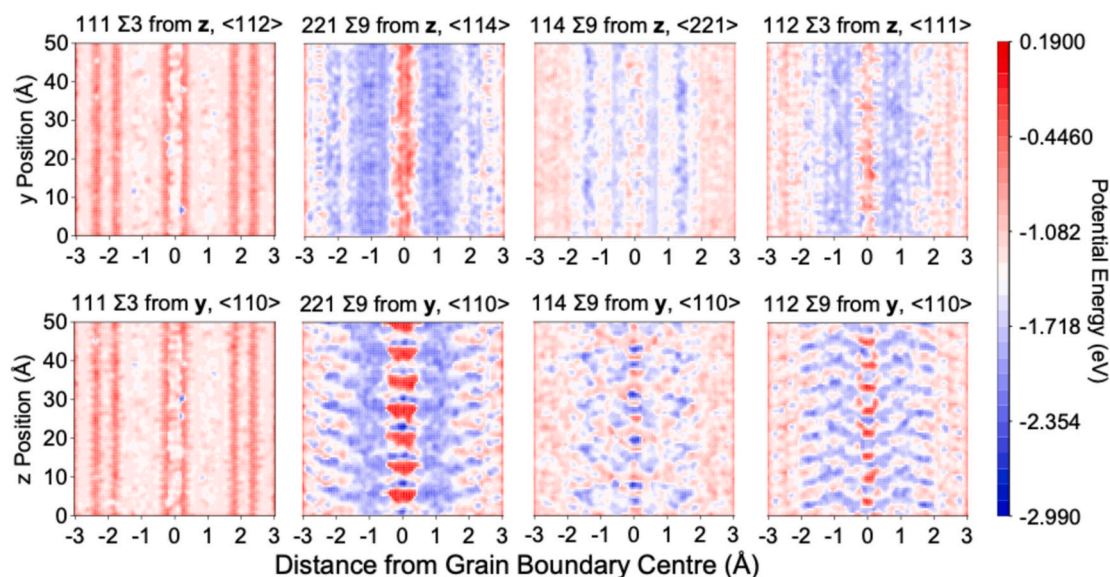


Fig. 3. Heatmaps of the potential energy of hydrogen placed in random positions and minimised for four diamond tilt grain boundaries. The top row of plots shows the grain boundary as if looking along the z direction, whereas the bottom along y . The same scale has been used on all the heatmaps to ensure they are comparable to one another. The z direction corresponds to $\langle 112 \rangle$, $\langle 114 \rangle$, $\langle 221 \rangle$ and $\langle 111 \rangle$ for the 111, 221, 114 and 112 GBs respectively, whereas all y directions were aligned with $\langle 110 \rangle$.

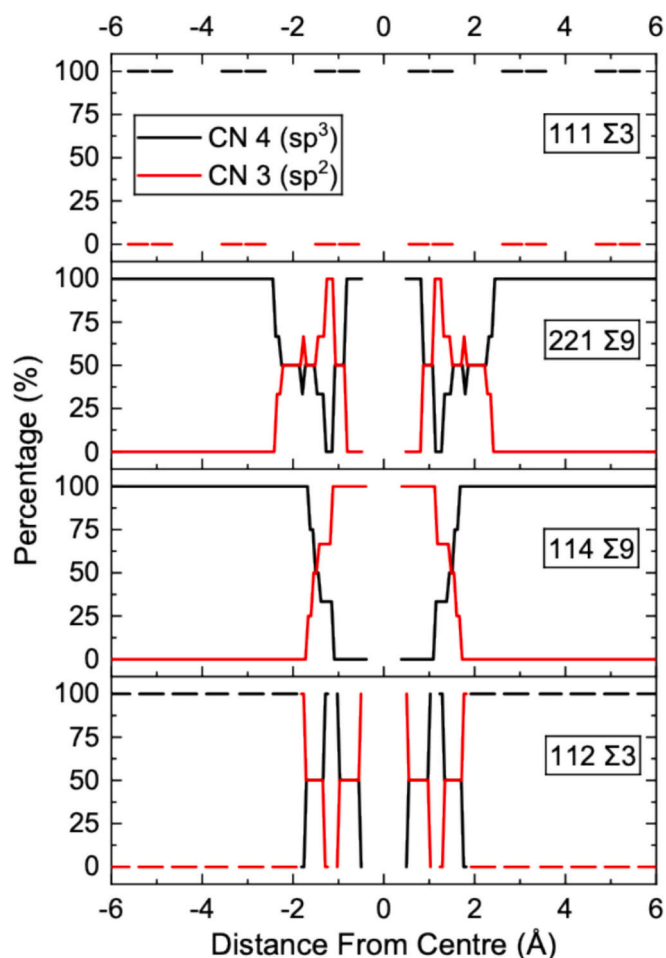


Fig. 4. sp^3 and sp^2 content across four tilt grain boundaries in diamond (111 $\Sigma 3$, 221 $\Sigma 9$, 114 $\Sigma 9$, 112 $\Sigma 3$) post energy minimisation. Coordination numbers (CN) of 3 and 4 were classed as sp^2 and sp^3 respectively and taken as a percentage of all atoms in that position. Gaps in data are a result of atomic layers leaving no carbon atoms in these positions. No sp^1 (CN 2) was found in any of the grain boundaries.

typically increase on the inclusion of additional atoms, changes in bond length and angle were also evaluated. For this, the carbon atom closest to each hydrogen atom was considered. The carbon carbon bond lengths and angles for this atom was compared to the structure without the addition of hydrogen.

3. Results and discussion

Fig. 1 shows the atomic structures of the grain boundaries, as well as the potential energy and final position of hydrogen placed within the simulation box in random positions and minimised. There are clear potential wells across grain boundaries in the 112, 114, and 221 GBs, resulting in hydrogen trapping within the grain boundary. This is in good agreement with physical expectation, as hydrogen within CVD diamond is typically concentrated to the grain boundaries [3]. The exception to this is the 111 GB, which shows a much less significant change across the grain boundary but more variation across the bulk. Both of these observations are a result of atomic alignment. (111) is a stable surface in diamond with atomic planes parallel to the surface, resulting in a coherent grain boundary without any significant deviation from the bulk structure. As the atomic planes are aligned with x across the grain boundary, collections of hydrogen in between atomic planes are observed at set x values, unlike in the other grain boundaries where atomic layers do not align with the x and the hydrogen trapped between

layers is averaged across atomic layers. This can be seen in Fig. 1a where the peaks in hydrogen correspond to the gaps between atomic layers. The average potential energy of hydrogen within the bulk regions was very consistent between the different orientations - all giving values of -1.08 eV to two decimal places with an average across the four structures of -1.0819 ± 0.0008 eV. Therefore, the hydrogen potential energy within bulk regions is largely independent of orientation as should be the case.

A consequence of this hydrogen trapping is the observation of anisotropic diffusion within the grain boundary, where hydrogen within grain boundaries preferentially diffuses within the grain boundary plane as opposed to drifting into the bulk. This can be seen in Fig. 2. For perfect diamond and the 111 GB, x , y and z components are approximately equal, suggesting no preferential direction of travel and isotropic diffusion. The same cannot be said for the three other grain boundaries, which present negligible diffusion in the x direction (across the grain boundary). In the 221 GB, the y component dominates. This direction aligns with $\langle 110 \rangle$, where clear channels can be seen in the grain boundary (see Fig. 1), offering preferential diffusion in comparison to the other directions. The isotropic diffusion observed for perfect diamond suggests no preferential diffusion in $\langle 110 \rangle$, meaning the larger channels present in the grain boundary are required. Although the 114 GB does show some displacement in the z direction (also within the grain boundary plane) this does not display a steady increase, suggesting atoms may have moved in this direction into channels which they then diffuse along in y . The 112 GB shows a gradual increase in displacement for both y and z directions, suggesting hydrogen is trapped within the grain boundary but able to move in both directions within.

Channels were explored further by plotting Fig. 3, which maps out the potential energy in two dimensions across the grain boundaries using the same data as presented in Fig. 1. It would be expected that regions of high contrast (indicating a significant difference in potential energy) should result in restricted diffusion. At a distance of ± 1 Å from the centre of the 221 GB, there are seemingly unobstructed low energy regions along the z direction. As very little diffusion was observed in this direction, it would suggest the fast diffusion in y is instead a result of areas of low energy along the centre of grain boundary. These are separated by high potential regions preventing diffusion in z and offer very effective channels for hydrogen transport. Similarly, the 114 GB also has its lowest energy points along the centre of the grain boundary. However, as other channels are present throughout this grain boundary, it is hard to determine whether these central channels are dominating. The regions of higher energy separating regions of lower energy along z result in more dominant diffusion along y . The contrast between these regions is less distinct than those in the 221 GB and some movement in y was initially observed of hydrogen moving into these channels. The 112 GB gave almost equal diffusion within the grain boundary. Although channels are visible in the y direction, the regions of high energy that separate them along z are less distinct than the 221 and 114 GBs, allowing some diffusion to occur in this direction. The 111 GB presents with a much more homogeneous potential energy with the only variation corresponding to atomic layers, resulting in the observed isotropic diffusion.

Hydrogen trapping within the grain boundary is thought to be a result of the increased sp^2 nature compared to the bulk. This can be seen in Fig. 4 which presents coordination number as a percentage across the grain boundaries. Within the 112, 114 and 221 GBs, a clear increase in sp^2 and decrease in sp^3 can be observed. The same cannot be said for the coherent 111 GB, in which only sp^3 is present throughout - in good agreement with physical expectations [9,23]. Hydrogen position peaks in Fig. 1 broadly align with peaks in sp^2 seen in Fig. 4. The double peak in hydrogen position in the 112 GB aligns with the double peak in sp^2 carbon within the grain boundary, the single peak in the 114 GB is comparable to its sp^2 content and the increase in sp^3 at the centre of the 221 GB gives an increase in potential energy and reduction in hydrogen occupation. This could simply be a result of the lower atom density

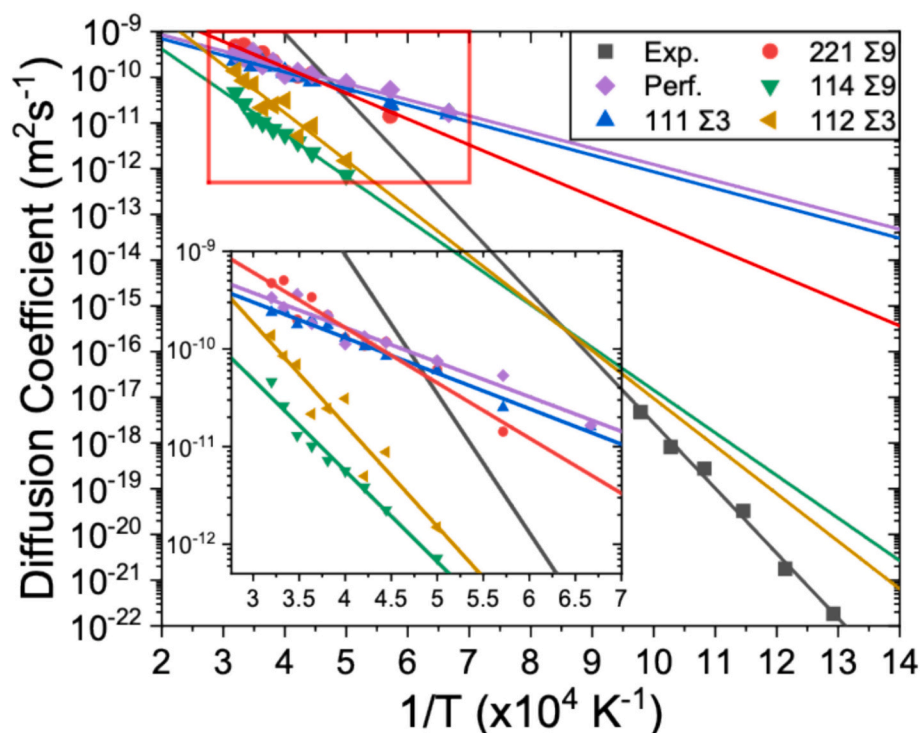


Fig. 5. Diffusion coefficients as a function of inverse temperature for various diamond structures. Miller indices in the legend give the direction of the tilt grain boundary modelled, data from these simulations have been plotted alongside values for perfect diamond (*Perf.*) which contained no grain boundary (simulating bulk diamond) and experimental values (*Exp.*) of polycrystalline diamond taken from [28]. The log of the diffusion coefficients have been fitted with a linear fit to give activation energies, E_A , in Table 1.

Table 1

Activation energies and preexponential factors as determined in Fig. 5. Experimental values taken from [28].

	D_0 (m^2s^{-1})	E_A (eV)
Experimental	2.6×10^{-4}	2.8 ± 0.2
Perfect (Bulk)	4.3×10^{-9}	0.70 ± 0.06
111 $\Sigma 3$	3.7×10^{-9}	0.72 ± 0.03
221 $\Sigma 9$	3.0×10^{-8}	1.1 ± 0.1
114 $\Sigma 9$	3.0×10^{-8}	1.9 ± 0.1
112 $\Sigma 3$	2.5×10^{-7}	2.1 ± 0.2

offering more positions for the hydrogen to sit and giving lower coordination numbers. However, in contrast to what is typically observed in crystalline solids, most grain boundaries presented higher activation energies than the bulk (or perfect diamond) as can be.

seen in Fig. 5 and Table 1. This behaviour would not be expected if diffusion was solely dictated by atomic density. Lower atomic density in grain boundaries would be expected to enhance diffusion compared to the bulk as seen in other crystalline solids. The difference is the type of bonding present in the covalently bonded carbon. On the inclusion of hydrogen into the grain boundary, hydrogen can form $\text{sp}^3\text{C-H}$ bonds with the sp^2 carbon present [24–26] resulting in restricted diffusion compared to the bulk where sp^3 carbon dominates and hydrogen occupies interstitial positions [3]. Formation of these more stable bonds will also contribute to the hydrogen trapping. For other diffusing species which cannot form covalent bonds with carbon, diamond grain boundaries have demonstrated preferential diffusion compared to the bulk [27], indicating the type of bonding is playing a role.

Experimental results for PC CVD diamond (taken from [28]) align best with 112 and 114 GBs both in terms of activation energy and diffusion coefficients at lower temperatures. As the experimental values are combination of bulk and grain boundary contributions, these results suggest the higher concentration of hydrogen within grain boundaries

and the restricted diffusion of this hydrogen is dominating, despite bulk regions making up a far greater proportion of polycrystalline diamond. As observed throughout the results presented here, the lack of a distinct grain boundary for the 111 GB resulted in very similar behaviour to perfect diamond. Although the 221 GB gave similar diffusion coefficients to perfect diamond and the 111 GB, the activation energy was still notably higher. As discussed, the diffusion within this grain boundary is thought to be dominated by hydrogen moving through low energy channels along the centre of the grain boundary. This channeling effect, as well as the presence of sp^3 carbon at the centre of this grain boundary (see Fig. 4) explains why the 221 GB presents with faster diffusion compared to the 114 and 112 GBs.

Bond length and angle distributions presented in Fig. 6 highlights the lack of deviation of the 111 GB from the perfect diamond structure, with both bond length and angle distributions presenting single values at 1.545 Å and 109.5° respectively. CN 4 carbon in the other grain boundaries showed some variation but distributions were centred about perfect diamond values. Where CN 3 carbon is present (for 221, 114 and 112 GBs), bond lengths are mostly shorter than CN 4 values. All three grain boundaries gave bond lengths in the 1.49–1.53 Å range, which align well with the range given for planar sp^3 - sp^2 bonding in [4] and is likely a result of bulk sp^3 carbon bonding to sp^2 carbon within the grain boundary. Bond lengths around 1.40–1.42 Å present for the 114 and 112 GB could indicate the presence of some pure $\text{sp}^2\text{C-C}$ bonds. The extreme high and low values present for the 114 GB are likely to be a result of the cut off used when determining coordination number. The bond lengths at 1.7 Å are unlikely to be physical, and instead could indicate some presence of sp^1 carbon as, if a shorter cutoff was used, these would not be counted and the carbon atom would be classed as CN 2/ sp^1 . The presence of sp^1 would also explain the bond length values of <1.4 Å.

Similarly, bond angles present consistent distributions around 109.5° for CN 4 carbon, and generally larger angles for CN 3 carbon. Here, only the 114 GB presents evidence of pure $\text{sp}^2\text{C-C}$ bonding, with

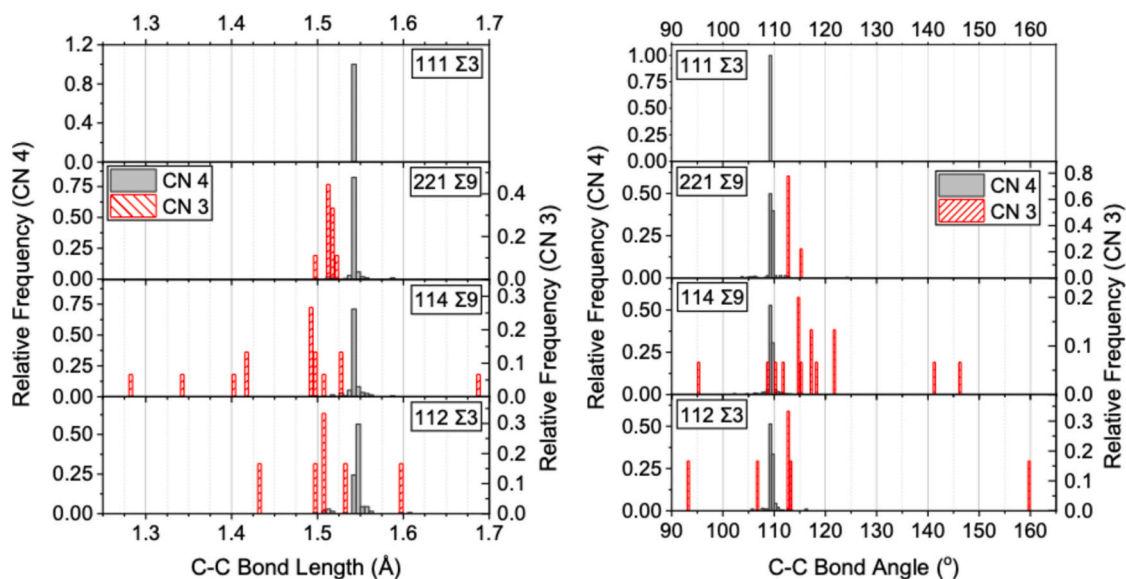


Fig. 6. Histograms comparing the bond lengths and angles for carbon bonds within a supercell containing the specified grain boundary post energy minimisation. CN 3/4 refers to the coordination number of the carbon atom. Perfect diamond effectively gave single values (of 1.545 Å and 109.5°) as seen for 111 Σ 3.

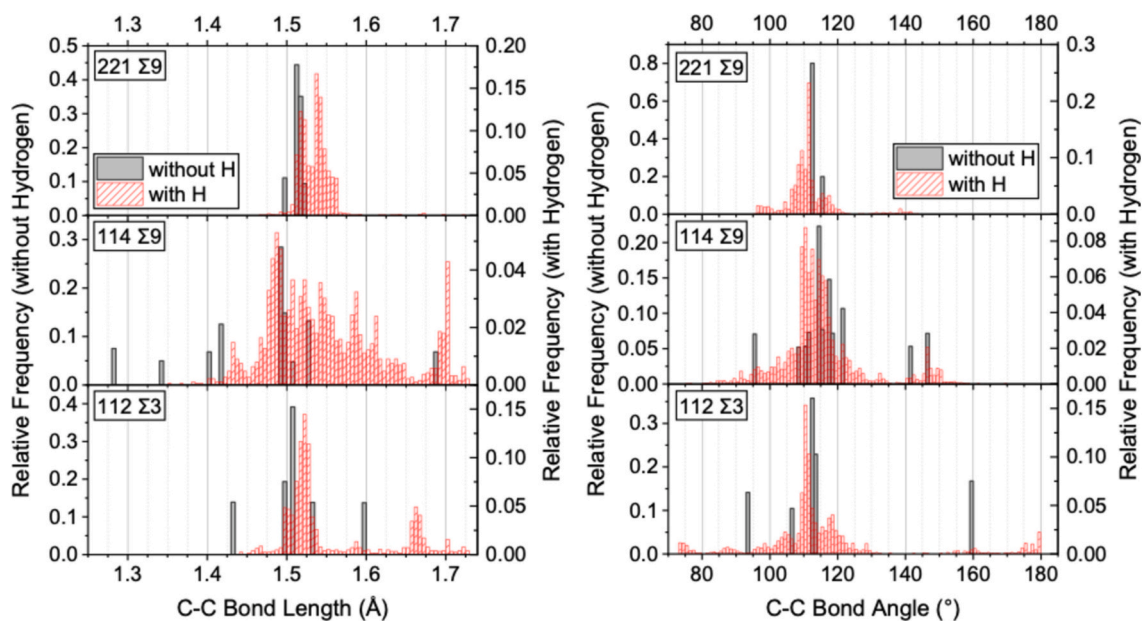


Fig. 7. Change in carbon bond length and angle from the inclusion of hydrogen atoms into the grain boundary post energy minimisation. Data shown only includes the carbon atoms closest to each hydrogen atom and only carbon atoms which went from a coordination number of 3 to 4 when the hydrogen was added.

bond angles around 120°. Although CN 3 carbon did give some bond angles <120°, generally, bond angles were higher than CN 4 carbon as would be expected for carbon with fewer nearest neighbours.

Upon adding hydrogen to the grain boundary many atoms presented an increase in coordination number as to be expected. The exception to this is when the presence of the hydrogen has pushed a carbon atom beyond the cutoff distance, resulting in no increase in coordination number. This scenario was more common for CN 4 carbon. It can be challenging to conclude whether an increase in coordination number is a true indicator of the sp^2 going to sp^3 C-H bonding as suggested in this work, as such, changes in bond length and angle were also considered.

Changes in bond length and angle on the inclusion of hydrogen can be seen in Fig. 7. Here, only data from the carbon atom closest to each hydrogen atom have been considered and only carbon that displayed an increase in coordination number from 3 to 4 (sp^2 to sp^3). As perfect

diamond and the 111 GB contained no sp^2 , these structures contained no carbon atoms that fulfilled these criteria. For all the grain boundaries with sp^2 , there is a reduction in the short bond lengths associated with sp^2 and sp^1 carbon on the inclusion of hydrogen. The 221 GB gives a clear peak at bond lengths that align well with sp^3 bonding, offering a good indication that sp^3 C-H may be forming. Similarly, adding hydrogen to the 112 GB removed the peak at 1.43 Å and shifted the most predominant peak to around 1.52 Å. Although this length is 0.025 Å shorter than seen for pure sp^3 , this increase still could indicate the presence of sp^3 C-H. The 114 GB gave a much broader distribution of bond lengths once the hydrogen was added, but again there was a general increase in bond length with the shortest values being lost. For this grain boundary in particular, the inclusion of hydrogen seems to result in a much more significant deviation from the initial structure and a general increase in disorder. This is despite the number of hydrogen atoms added being

halved and the number of repeated calculations being increased to try and improve the clarity of the data. The 114 GB is the only grain boundary with no sp^3 at the centre of the grain boundary, and the only one whose bond lengths suggested the presence of sp^1 . This indicates more space is present within the grain boundary, allowing movement of carbon atoms and an increase in disorder on the inclusion of hydrogen.

There are more similarities between the grain boundaries when looking at the bond angles. Once hydrogen was added, the bond angle distributions reduced to a peak centred about 110° - in good agreement with what would be expected for the formation of sp^3C-H . The 114 GB in particular showed a notable reduction in 120° bond angles which are commonly associated with sp^2 carbon.

Overall, in grain boundaries containing sp^2 carbon, changes in bond length and angle on the inclusion of hydrogen are present which could be associated with a transition from sp^3 - sp^2 to sp^3C-H . The 221 GB gave the clearest evidence of this, whereas the 114 GB had a more general increase in disorder. The formation of sp^3C-H is thought to contribute to restricted diffusion observed in these grain boundaries compared to perfect diamond or the 111 GB. Despite the 221 GB showing the clearest indication of sp^3C-H forming, it gave the fastest diffusion and lowest activation energy of the grain boundaries containing sp^2 carbon. This is thought to be a result of the low energy channels present in this grain boundary, as well as the sp^3 carbon aligned with these channels. However, the formation of sp^3C-H with sp^2 outside of these channels, still resulted in a higher activation energy than perfect diamond. The 112 GB showed evidence of sp^3C-H forming and minimal channelling effects were present, resulting in slow overall diffusion. It cannot be said definitively that sp^3C-H formed in the 114 GB due to the broad bond length distribution on the addition of hydrogen, however, some evidence of this was present. There were some channels observed for this grain boundary, but the changes in bond length and angle indicate notable deviation from the initial structure and such disorder is likely to outweigh the impact of these and restrict the overall diffusion rates.

4. Conclusion

Molecular dynamics simulations were performed to explore hydrogen diffusion in diamond grain boundaries. Four common grain boundaries were replicated from TEM images from [7], and it was found that all but the 111 GB had a significant potential well across the grain boundary. This resulted in hydrogen trapping, in good agreement with expected physical behaviour. Anisotropic diffusion was also observed in these grain boundaries with hydrogen preferentially travelling along channels in (110) but only within grain boundaries. The exception to this was the 111 GB, which gave isotropic diffusion and generally behaved much more similarly to the perfect diamond.

Overall diffusion rates are thought to be influenced by sp^2 content and channels present within the grain boundaries. When present, sp^2 carbon resulted in restricted diffusion from the formation of sp^3C-H bonds rather than the interstitial positions occupied in the bulk [3,24–26]. In contrast, the presence of channels and sp^3 carbon in some grain boundaries acted to increase diffusion rates. Evidence of the formation of sp^3C-H with sp^2 carbon was observed through consideration of bond length and angle distributions.

Diffusion characteristics will dictate the impact annealing and other similar treatments will have on the hydrogen content of diamond. The conclusions that can be drawn regarding this from the results presented here are limited without an understanding of the distribution of different grain boundaries present. For tilt grain boundaries rotated about (110), these results would suggest hydrogen would remain within grain boundaries during heat treatments, whereas hydrogen in bulk regions is more likely to be removed or become trapped in grain boundaries. Different grain boundaries clearly present different degrees of hydrogen trapping and diffusion rates, meaning the hydrogen content is likely to vary significantly between grain boundaries especially post heat treatment. Atomic alignment in (110) results in significant channels within

the tilt grain boundaries. This may not be the case for (100) and (111), so more work would be needed to draw conclusions for other diamond orientations.

CRediT authorship contribution statement

J.A. Pittard: Writing – review & editing, Writing – original draft, Investigation, Formal analysis, Data curation. **M.Y. Lavrentiev:** Writing – review & editing, Supervision, Funding acquisition, Formal analysis, Data curation. **N.A. Fox:** Writing – review & editing, Supervision.

Declaration of competing interest

The authors declare that they have no known competing financial interests or personal relationships that could have appeared to influence the work reported in this paper.

Acknowledgements

We acknowledge the support of EPSRC, UKAEA and funding by the RCUK Energy Programme (Grant No. EP/W006839/1). This work was carried out using the computational facilities of the Advanced Computing Research Centre, University of Bristol – <http://www.bris.ac.uk/acr> and the Cambridge Service for Data Driven Discovery (CSD3) – <https://www.csd3.cam.ac.uk>.

Data availability

Data will be made available on request.

References

- [1] P.W. May, Diamond thin films: a 21st-century material, *Trans. R. Soc. Lond. A* 358 (2000) 473–495.
- [2] M. Shimada, 6.08 - tritium transport in fusion reactor materials, in: *Comprehensive Nuclear Materials*, 2nd edition, Elsevier, Oxford, 2020, pp. 251–273.
- [3] J.P. Goss, R. Jones, M.I. Heggie, C.P. Ewels, P.R. Briddon, S. Oberg, Theory of hydrogen in diamond, *Phys. Rev. B Condens. Matter* 65 (2002) 1–13.
- [4] P. Zapol, M. Sternberg, L.A. Curtiss, T. Frauenheim, D.M. Gruen, Tight-binding molecular-dynamics simulation of impurities in ultrananocrystalline diamond grain boundaries, *Phys. Rev. B Condens. Matter* 65 (2002) 454031–4540311.
- [5] C. Baruffi, C. Brandl, On the structure of (111) twist grain boundaries in diamond: atomistic simulations with Tersoff-type interatomic potentials, *Acta Mater.* 215 (2021) 117055.
- [6] O.A. Shenderova, D.W. Brenner, L.H. Yang, Atomistic simulations of structures and mechanical properties of polycrystalline diamond: symmetrical (001) tilt grain boundaries, *Phys. Rev. B Condens. Matter* 60 (1999) 7043–7052.
- [7] H. Sawada, H. Ichinose, M. Kohyama, Atomic structure of the σ_3 and σ_9 grain boundaries in CVD diamond film, *Scr. Mater.* 51 (2004) 689–692.
- [8] W. Luyten, G.V. Tendeloo, S. Amelincx, J.L. Collins, Electron microscopy study of defects in synthetic diamond layers, *Philos. Mag.* A 66 (1992) 899–915.
- [9] O.R. Monteiro, Structural defects and sp^2 localization in CVD diamond, *J. Mater. Sci.* 54 (2019) 2300–2306.
- [10] A.H. King, F. Chen, L. Chang, J.J. Kai, Toward understanding polycrystalline aggregate structure: analysis of a twin intersection and the interactions between interfaces in diamond, *Interface Sci.* 5 (1997) 287–303.
- [11] O.A. Shenderova, D.W. Brenner, Atomistic simulations of structures and mechanical properties of (011) tilt grain boundaries and their triple junctions in diamond, *Phys. Rev. B Condens. Matter* 60 (1999) 7053–7061.
- [12] D. Shechtman, J. Hutchison, L. Robins, E. Farabaugh, A. Feldman, Growth defects in diamond films, *J. Mater. Res.* 8 (1993) 473–479.
- [13] P. in 't Veld, S.J. Plimpton, G.S. Grest, Accurate and efficient methods for modeling colloidal mixtures in an explicit solvent using molecular dynamics, *Comput. Phys. Commun.* 179 (2008) 320–329.
- [14] A.P. Thompson, H.M. Aktulga, R. Berger, D.S. Bolintineanu, W.M. Brown, P. S. Crozier, et al., LAMMPS - a flexible simulation tool for particle-based materials modelling at the atomic, meso, and continuum scales, *Comput. Phys. Commun.* 271 (2022) 108171.
- [15] D.W. Brenner, O.A. Shenderova, J.A. Harrison, S.J. Stuart, B. Ni, S.B. Sinnott, A second-generation reactive empirical bond order (REBO) potential energy expression for hydrocarbons, *J. Phys. Condens. Matter* 14 (2002) 783–802.
- [16] D.W. Brenner, Empirical potential for hydrocarbons for use in simulating the chemical vapor deposition of diamond films, *Phys. Rev. B Condens. Matter* 42 (1990) 9458–9471.
- [17] S.J. Stuart, A.B. Tutein, J.A. Harrison, A reactive potential for hydrocarbons with intermolecular interactions, *J. Chem. Phys.* 112 (2000) 6472–6486.

- [18] P. Steneteg, V. Chirita, N. Dubrovinskaia, L. Dubrovinsky, I.A. Abrikosov, Missing-atom structure of diamond $\Sigma 5$ (001) twist grain boundary, *Phys. Rev. B Condens. Matter* 84 (2011) 144112.
- [19] S.V. Altham, P.D. Haynes, K. Kaski, A.P. Sutton, Are the structures of twist grain boundaries in silicon ordered at 0 K? *Phys. Rev. Lett.* 96 (2006) 055505.
- [20] T. Watanabe, B. Ni, S.R. Phillpot, P.K. Schelling, P. Keblinski, Thermal conductance across grain boundaries in diamond from molecular dynamics simulation, *J. Appl. Phys.* 102 (2007) 063503.
- [21] A. Stukowski, Visualization and analysis of atomistic simulation data with OVITO—the open visualization tool, *Model. Simul. Mater. Sci. Eng.* 18 (2009) 015012.
- [22] L. Li, M. Xu, W. Song, A. Ovcharenko, G. Zhang, D. Jia, The effect of empirical potential functions on modeling of amorphous carbon using molecular dynamics method, *Appl. Surf. Sci.* 286 (2013) 287–297.
- [23] H. Ichinose, M. Nakanose, Atomic and electronic structure of diamond grain boundaries analyzed by HRTEM and EELS, *Thin Solid Films* 319 (1998) 87–91.
- [24] M. Sasaki, Y. Morimoto, H. Kimura, K. Takahashi, K. Sakamoto, T. Imai, et al., Energetic deuterium and helium irradiation effects on chemical structure of CVD diamond, *J. Nucl. Mater.* 329-333 (2004) 899–903.
- [25] H. Kimura, M. Sasaki, Y. Morimoto, T. Takeda, H. Kodama, A. Yoshikawa, et al., Thermal desorption behavior of deuterium implanted into polycrystalline diamond, *J. Nucl. Mater.* 337-339 (2005) 614–618.
- [26] N. Nishikawa, Evidence of hydrogen termination at grain boundaries in ultrananocrystalline diamond/hydrogenated amorphous carbon composite thin films synthesized via coaxial arc plasma, *J. Vac. Sci. Technol. B* 38 (2020) 062803.
- [27] D. Berman, S.A. Deshmukh, B. Narayanan, S.K. Sankaranarayanan, Z. Yan, A. A. Balandin, A. Zinovev, D. Rosenmann, A.V. Sumant, Metal-induced rapid transformation of diamond into single and multilayer graphene on wafer scale, *Nat. Commun.* 7 (2016) 12099.
- [28] D.J. Cherniak, E.B. Watson, V. Meunier, N. Kharche, Diffusion of helium, hydrogen and deuterium in diamond: experiment, theory and geochemical applications, *Geochim. Cosmochim. Acta* 232 (2018) 206–224.